Denervation protects limbs from inflammatory arthritis via an impact on the microvasculature

Lars Stangenberg[a,1], Dalia Burzyn[b], Bryce A. Binstadt[b,2], Ralph Weissleder[a], Umar Mahmood[a,3], Christophe Benoist[b], and Diane Mathis[b,4]

[a]Center for Systems Biology, Massachusetts General Hospital, Harvard Medical School, Boston, MA 02114; and [b]Division of Immunology, Department of Microbiology and Immunobiology, Harvard Medical School, Boston, MA 02115

Contributed by Diane Mathis, June 10, 2014 (sent for review May 22, 2014)

Two-way communication between the mammalian nervous and immune systems is increasingly recognized and appreciated. An intriguing example of such crosstalk comes from clinical observations dating from the 1930s: Patients who suffer a stroke and then develop rheumatoid arthritis atypically present with arthritis on only one side, the one not afflicted with paralysis. Here we successfully modeled hemiplegia-induced protection from arthritis using the K/BxN serum-transfer system, focused on the effector phase of inflammatory arthritis. Experiments entailing pharmacological inhibitors, genetically deficient mouse strains, and global transcriptome analyses failed to associate the protective effect with a single nerve quality (i.e., with the sympathetic, parasympathetic, or sensory nerves). Instead, there was clear evidence that denervation had a long-term effect on the limb microvasculature: The rapid and joint-localized vascular leak that typically accompanies and promotes serum-transferred arthritis was compromised in denervated limbs. This defect was reflected in the transcriptome of endothelial cells, the expression of several genes impacting vascular leakage or transendothelial cell transmigration being altered in denervated limbs. These findings highlight a previously unappreciated pathway to dissect and eventually target in inflammatory arthritis.

inflammation | nervous system | vascular system | autoantibody

It has long been recognized that immune and inflammatory processes can be influenced by signals from the nervous system (1). For example, neuroendocrine hormones have well-known anti-inflammatory activities, first documented for corticosteroids in the arthritis context (2). Subsequently, motor neurons, the sympathetic nervous system (SNS), the parasympathetic nervous system (PNS), and sensory fibers have all been documented to modulate inflammation (3–5).

A striking example of nervous–immune system interaction comes from clinical observations made decades ago. As early as 1935, it was reported that patients who suffered a stroke and then developed rheumatoid arthritis (RA), often years after the neurologic insult, had an atypical disease presentation: Instead of the inflammatory symmetry typical of RA, only neurologically intact limbs developed joint inflammation (6). Later, this effect of central denervation was extended to peripheral denervation: Patients who were hemiplegic subsequent to polio or syphilis developed an analogous asymmetric arthritis (7, 8).

We set out to dissect this clinical phenomenon mechanistically by exploiting the power of the K/BxN T-cell receptor transgenic mouse model of inflammatory arthritis (9, 10). This model is particularly useful because of its easily distinguishable initiation and effector stages. The initiation phase relies primarily on the adaptive immune system. T lymphocytes displaying the transgene-encoded T-cell receptor recognize a self-peptide derived from GPI presented by the major MHC class II molecule, Ag7; these autoreactive T cells provide exceptionally effective help to GPI-specific B cells, resulting in massive, IL-17–dependent production of anti-GPI autoantibodies (autoAbs), primarily of the IgG1 isotype. The effector phase, which can be mimicked conveniently by transfer of serum from K/BxN into standard mice, is executed primarily by innate immune system players. GPI:anti-GPI immune complexes initiate a self-sustaining inflammatory response that mobilizes mast cells, neutrophils, perhaps macrophages, the alternative pathway of complement, Fc gamma receptors (FcγRs), TNF-α, IL-1, and others.

It proved possible to model hemiplegia-induced protection from arthritis in the K/BxN serum-transfer system: Serum recipients that had undergone unilateral transection of the sciatic and femoral nerves developed arthritis only in the paw on the innervated side. This finding prompted us to assess the roles of diverse elements of the nervous and allied systems in arthritis progression subsequent to serum transfer. Results from experiments using genetically deficient mouse strains and pharmacological inhibitors were unable to implicate a particular nerve quality but did point to a role for endothelial cells of the microvasculature. In accord, the endothelial cell transcriptomes of denervated and innervated ankles from K/BxN serum-transferred mice differed substantially and suggestively.

Results

Establishment of a Mouse Model of Asymmetric Arthritis Subsequent to Unilateral Paralysis. To enable mechanistic dissection of the arthritis-protective effect of hemiplegia, we adapted the K/BxN serum-transfer system. The hindpaw on one side of 6- to 8-wk-old C57BL/6 (B6) mice was denervated by transection of both the sciatic and femoral nerves, and the contralateral limb underwent a sham operation. Typically 10 d later, K/BxN serum was injected

Significance

Individuals who suffer paralysis on one side of the body and then develop rheumatoid arthritis show joint inflammation only on the neurologically intact side. We successfully modeled hemiplegia-induced protection from arthritis by transferring arthritogenic serum from K/BxN mice into recipients that had undergone unilateral sciatic and femoral nerve transection. Protection from serum-transferred arthritis could not be achieved by inhibiting the sympathetic, parasympathetic, or sensory arms of the nervous system. However, nerve transection did inhibit the joint-localized, inflammation-enhancing vascular leak rapidly induced by arthritogenic immune complexes and suggestively altered the transcriptome of the ankle microvasculature.

Author contributions: L.S., D.B., B.A.B., R.W., U.M., C.B., and D.M. designed research; L.S., D.B., and B.A.B. performed research; D.B., B.A.B., R.W., U.M., C.B., and D.M. analyzed data; and D.B. and D.M. wrote the paper.

The authors declare no conflict of interest.

[1]Present address: Beth Israel Deaconess Medical Center, Harvard Medical School, Boston, MA 02215.

[2]Present address: Center for Immunology, University of Minnesota, Minneapolis, MN 55414.

[3]Present address: Department of Radiology, Massachusetts General Hospital, Harvard Medical School, Boston, MA 02114.

[4]To whom correspondence should be addressed. Email: dm@hms.harvard.edu.

This article contains supporting information online at www.pnas.org/lookup/suppl/doi:10.1073/pnas.1410854111/-/DCSupplemental.

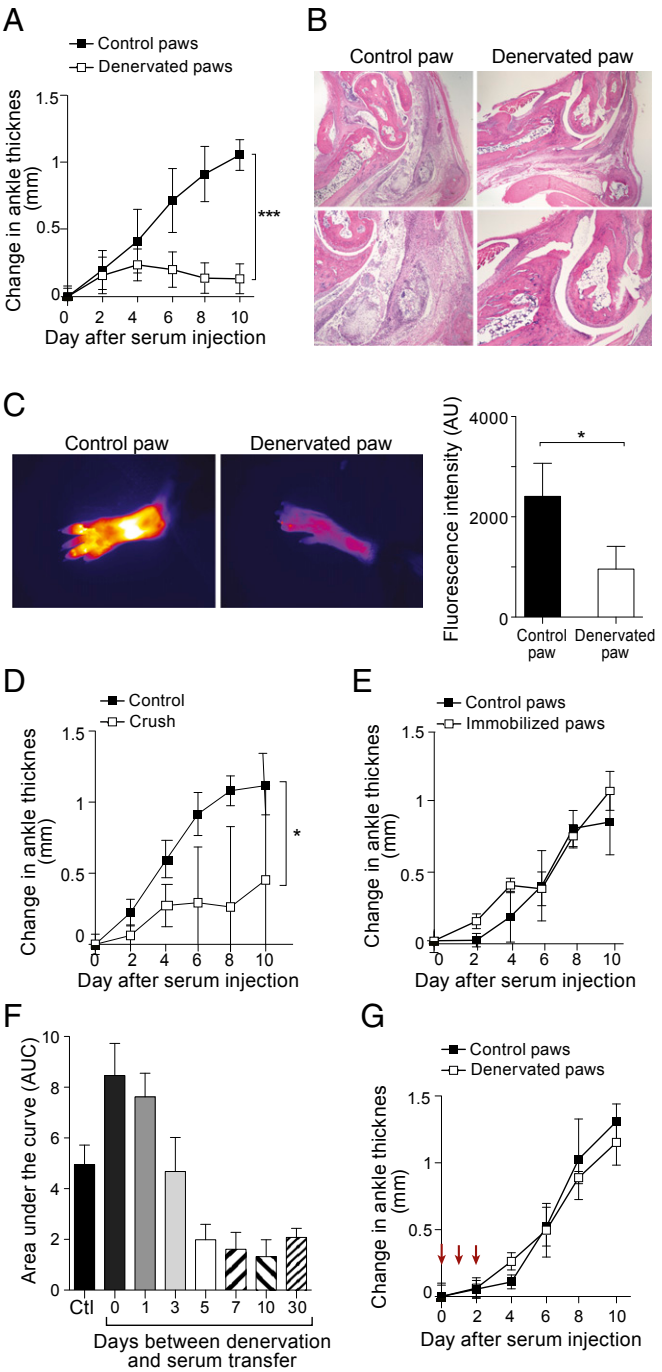

Fig. 1. Asymmetric arthritis after unilateral denervation. (*A*–*C*) B6 mice were subject to hindlimb denervation on one side and a sham operation on the other. Ten days later, they were injected with K/BxN serum (day 0), and arthritis was monitored over time by diverse assays. (*A*) Ankle swelling. Data shown are mean ± SD; ***$P < 0.001$ determined by Student *t* test; $n = 4$. (*B*) Histology. Analyzed by H&E staining 10 d after serum injection. (Magnification: *Upper*, 2×; *Lower*, 10×.) (*C*) Real-time protease imaging. A fluorescent cathepsin-B–activatable probe (ProSense) was injected on day 9 and imaged on day 10 after serum injection. (*Left*) Examples of images obtained with 2.7× magnification and color-coded in ImageJ with Fire. (*Right*) Summary quantification. Data shown are mean ± SD; *$P < 0.05$, determined by Student *t* test; $n = 4$. (*D*) Crush injury. Rather than surgical denervation, hindlimbs were subject to a milder crush, injury. Arthritis was induced and assayed as in *A*. *$P < 0.05$; $n = 3$. (*E*) Joint immobilization. Rather than surgical denervation, hindlimb joints were splint-immobilized. Arthritis was induced as in *A*. $n = 3$. (*F*) Impact of time since denervation. As in *A*, except varying intervals between surgery and serum transfer were tested. Area under the curve values are plotted; full curves can be found in Fig. S1. Ctl, sham-operated control. Data are shown as mean ± SD; $n = 4$. (*G*) Reversal of arthritis protection. As in *A*, except that IL-1β was i.p. injected on days 0, 1, and 2 (arrows) vis-à-vis serum transfer. $n = 4$.

i.p., usually twice, 2 d apart, and inflammatory arthritis was assessed over time.

As anticipated, control paws showed a steady augmentation of ankle thickness over the 10-d observation period; in contrast, denervated paws exhibited the usual increase only until day 2, after which there was little additional ankle thickening (Fig. 1*A*). Histologic examination at day 10 revealed the expected severe inflammation of control paws: a massive influx of neutrophils in periarticular tissues and within the synovial space and synovial hypertrophy (Fig. 1*B*, *Left*). These abnormalities were almost completely absent in the denervated paws (Fig. 1*B*, *Right*). Cathepsin B activity, another marker of inflammatory arthritis (11), also was greatly reduced in denervated paws, as indicated by minimal cleavage of a cathepsin-sensitive fluorescent nanoparticle injected on day 10 and monitored by noninvasive imaging (Fig. 1*C*). Nerve-crush injury, more mild than nerve transection, afforded protection as well, although such protection appeared to be less robust than that resulting from severance of the nerves (Fig. 1*D*).

To assess the importance of motor function in the serum-transfer system, we evaluated the effect of immobilizing hindpaws by application of a splint. This procedure did not confer protection from arthritis (Fig. 1*E*), although it is difficult to ensure absolute immobilization using such a strategy.

There was an intriguing time-dependence to the effect of denervation on the development of arthritis in the serum-transfer model. Concurrent nerve transection and serum injection paradoxically resulted in increased ankle swelling on the denervated compared with the innervated side (Fig. 1*F* and Fig. S1). With increasingly longer intervals between surgery and arthritis induction, this proinflammatory response converted to an anti-inflammatory, arthritis-protective mode, which was maintained for more than 1 mo after denervation (Fig. 1*F* and Fig. S1).

Last, we wondered whether the denervation-induced block to arthritis progression is reversible. Injection of a bolus of IL-1β can bypass genetic resistance to the arthritogenic power of K/BxN serum (12). IL-1β, administered on three consecutive days at the time of serum injection, completely reversed the arthritis block in denervated limbs, driving disease to the same level as in the innervated counterparts (Fig. 1*G*).

Comparison of the Transcriptomes of Control and Denervated Ankles. For additional insight into the aborted arthritis induced in the denervated limbs, we turned to genome-wide transcriptome analysis. We began by identifying gene-expression differences in whole-ankle tissue dissected from denervated and sham-operated limbs, independent of the response to K/BxN serum. Even 10 d post-surgery, the ankle-tissue transcriptomes diverged extensively: 238 genes were up-regulated, and 364 genes were down-regulated by at least twofold in the denervated samples ($P < 10^{-4}$, by permutation analysis) (Fig. 2*A* and Tables S1 and S2). These changes reflected a number of pathways involved in tissue homeostasis and development (see Fig. 2*B* for top pathway "hits" from Ingenuity analysis and Tables S3 and S4 for the actual genes involved), but the identity of these pathways yielded no obvious explanations for the arthritis-protective effect. Not surprisingly, and reassuringly, the transcripts most underrepresented in the denervated tissue encoded many myelin- and muscle-associated proteins (Table S2).

Subsequently, we compared gene-expression profiles of ankle tissue from denervated and innervated limbs after the administration of K/BxN serum. The analysis was focused on day 4 after serum transfer because this time point was the first to show a difference in ankle thickness and therefore might provide clues

to early defective processes, before secondary effects set in. Again the transcriptomes of denervated vs. innervated ankle tissue diverged significantly: 136 were up-regulated, and 241 genes were down-regulated in the denervated samples ($P < 10^{-4}$, by permutation analysis) (Fig. 2*C*). Superimposing on this plot the sets of transcripts over- or underrepresented in the absence of serum challenge (red and blue in Fig. 2*A*) revealed that most of the differential expression on day 4 after serum administration carried over from the prechallenged state (day 0). Few immunity- or inflammation-related genes made the twofold cutoff, notably the gene encoding SAA-1 did, an acute-phase reactant whose levels mount in blood and synovial fluid of arthritic humans and rodents (13) (Tables S5 and S6).

Assessment of the Contribution of Diverse Nerve Types to K/BxN Serum-Transferred Arthritis. We then sought to identify the type (s) of nerve involved in this model of inflammatory arthritis. The arthritis-protective effect detailed above was conferred by transection of the femoral and sciatic nerves, severing a variety of nerve types: motor, sympathetic, possibly parasympathetic, and sensory. First, we examined the impact of the two components of the vegetative nervous system, the SNS and PNS. The SNS seems to exert pro- or anti-inflammatory activity depending on the context, typically promoting inflammation at the outset of an immune response and reining it in at later stages (14). For example, blockade of β2 sympathetic signaling delayed the onset of antigen-induced arthritis and reduced its severity (3), whereas sympathectomy performed late in the course of collagen-induced arthritis worsened disease manifestations (15). To test the influence of the SNS in the K/BxN serum-transfer system, we administered, along with the serum, a set of pharmacologic agents that operate by a diversity of mechanisms. Guanethidine, a nonactive competitive inhibitor of norepinephrine at the presynaptic terminal, did not impact joint swelling; 6-hydroxydopamine, a potent neurotoxin, similarly failed to have an effect, as did reserpine, an irreversible norepinephrine reuptake inhibitor (Fig. 3*A*).

The PNS and its main anatomic correlate, the vagus nerve, have been linked to several inflammatory processes, usually exerting a dampening effect. For example, increased vagus nerve activity attenuated systemic sepsis, reducing levels of proinflammatory cytokines such as TNF-α, IL-1, and IL-6, whereas vagotomy exacerbated disease (5). The vagus nerve's anti-inflammatory function is mediated through acetylcholine (Ach) and a specific nicotinic Ach receptor, nAchRa7, which is present on macrophages and links the nervous and immune systems (16). The PNS was interrogated both via pharmacological inhibition and in KO mice. Coadministration of K/BxN serum and hexamethonium, a nondepolarizing ganglionic blocker, actually enhanced joint swelling (Fig. 3*B*, *Left*). On the other hand, mecamylamine, a nonselective and noncompetitive antagonist of nAchRs, did not change the course of disease (Fig. 3*B*, *Left*). Neither of these compounds is truly selective for the PNS, however; both inhibit SNS function as well. Therefore, as an independent test of the role of the PNS, we transferred serum into mice with a null mutation for *nAchRa7*. Arthritis developed as usual in these recipients (Fig. 3*B*, *Right*).

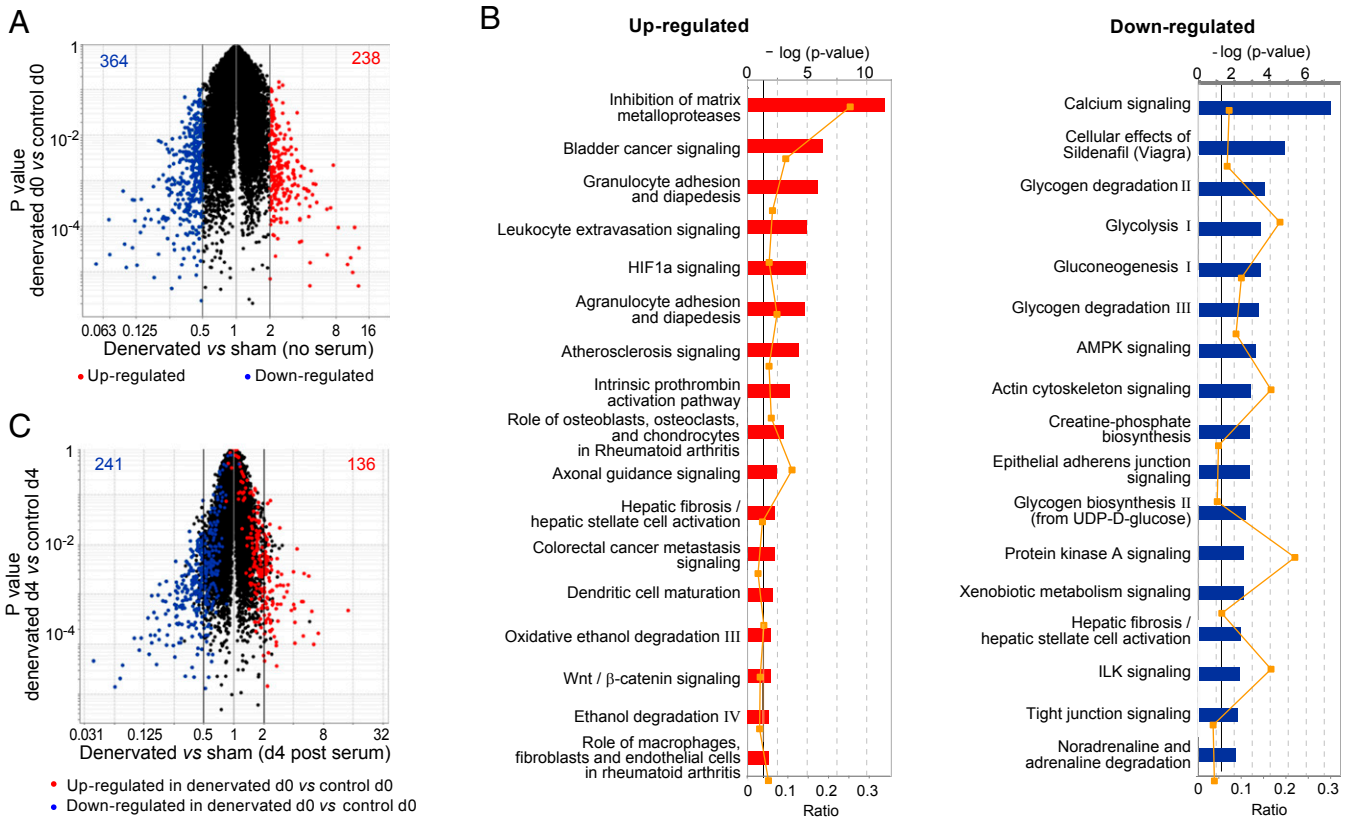

Fig. 2. Comparison of the transcriptomes of control and denervated ankles. Whole tissue from ankles of denervated or sham-operated limbs was dissected before or 4 d after induction of arthritis, and global gene expression was analyzed by microarray. (*A*) Volcano plot showing changes in gene expression induced by denervation in the absence of arthritis induction. (*B*) Canonical pathways (from Ingenuity) most enriched in sets of genes up- (*Left*) or down- (*Right*) regulated by denervation. The orange line indicates the ratio, calculated as the number of genes in a given pathway that meet cutoff criteria divided by total number of genes that make up that pathway. (*C*) Volcano plot comparing gene expression in denervated vs. control ankle tissue at day 4 after arthritis induction. Highlights represent genes up- (red) or down- (blue) regulated in denervated ankles in the absence of serum transfer (from *A*).

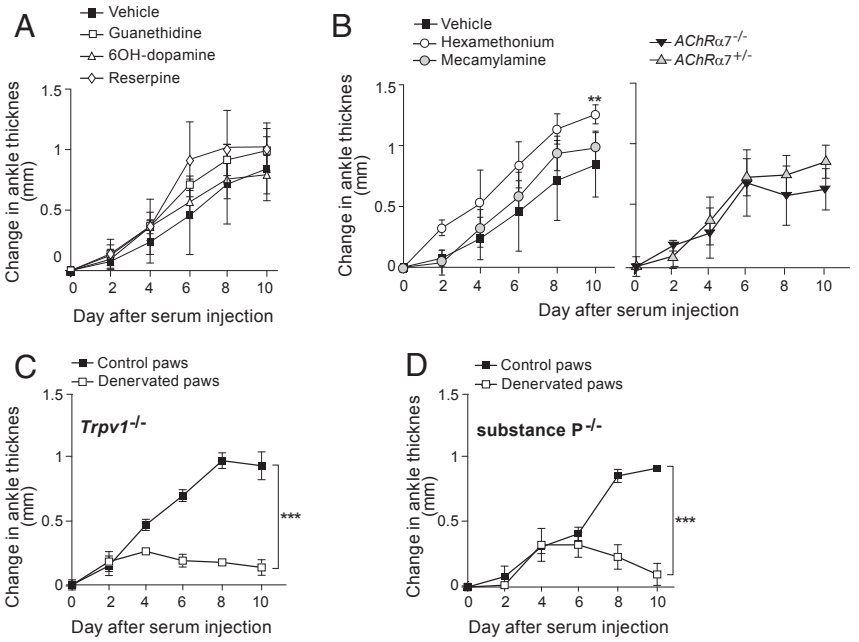

Fig. 3. Evaluation of the roles of various nerve types. (*A* and *B*) Role of the vegetative nervous system in K/BxN serum-transferred arthritis. Arthritis was induced and assayed in innervated limbs as in Fig. 1*A*. Pharmacological inhibitors of the SNS (*A*) or PNS (*B*, *Left*) were administered beginning on day 0, at the time of serum transfer. (*B*, *Right*) The response of *AchRα7*-KO mice and control littermates was tested. $^{**}P < 0.01$. (*C* and *D*) Role of sensory nerves in serum-transferred arthritis. Arthritis was induced and assayed in denervated or innervated hindlimbs as in Fig. 1*A*. The response of mice genetically deficient in Trpv-1 (*C*) or substance P (*D*) that had or had not been denervated was tested. $^{***}P < 0.001$; $n = 3$ for each condition.

Sensory fibers also can play an active role in inflammatory processes, expressing a variety of relevant receptors on their endings, including Toll-like, cytokine, prostaglandin, and catecholamine receptors (14). The transient receptor potential vanilloid cation channel 1 (TRPV1) is a proinflammatory nerve-fiber receptor that is activated by capsaicin (4). TPRV1 and like receptors are thought to sense activation of the immune system and to report the information to higher nerve centers in the spinal cord and brain. Subsequently, they release neuropeptides such as substance P and calcitonin gene-related peptide-1 (CGRP-1), which have powerful vasodilatory and chemotactic properties and thereby can prime the local environment for an inflammatory response (17, 18). To assess the influence of sensory nerves on K/BxN serum-transferred arthritis, we tested mice bearing a null mutation for TRPV1 or for substance P. Transfer of serum into each of these KO strains could provoke inflammatory arthritis with the usual course, and disease could be inhibited by denervation (Fig. 3 *C* and *D*).

Demonstration of Effects on the Microvasculature. We showed previously that K/BxN serum-transferred arthritis induces and depends on a rapid and joint-localized increase in microvascular permeability, a process that requires histamine and serotonin (19). There are manifold links between the nervous and vascular systems: For example, VEGF, a major stimulant of angiogenesis, also promotes axon growth (20); the SNS and PNS control cardiovascular parameters such as blood pressure and heart rate; and the neurovascular unit, a term encompassing endothelial cells, neurons, astrocytes, pericytes, and extracellular matrix, is increasingly recognized as central to neurodegenerative diseases (21). Hence, we quantified vascular leakage in denervated and sham-operated limbs of K/BxN-serum recipients. Using a noninvasive, real-time method for visualizing the vasculature of live mice via confocal microscopy of a long-circulating intravascular imaging probe (19), we found a clear reduction and delay in the vessel leakage that typically occurs minutes after serum injection (Fig. 4 *A* and *B*). Because systemic administration of histamine or serotonin had been shown previously to trigger analogous joint-localized vasopermeability in limbs of standard mice, i.e., to mimic the effect of GPI:anti-GPI immune complexes, we checked whether this triggering also occurred in denervated limbs. It did not, suggesting a defect in endothelial cell sensing (Fig. 4*C*).

Given the clear impact of denervation on the vasculature of serum-transferred mice and the lack of reversal by vasoactive amines, we looked for mechanistic clues in the transcriptomes of hindpaw endothelial cells. Tie2-GFP mice, in which endothelial cells are fluorescently tagged, were subjected to denervation or a sham operation. After 10 d, hindpaw endothelial cells were purified by flow cytometry, RNA was isolated, and gene expression was profiled using Affymetrix microarrays. To focus on genes relevant to vascular permeability, we generated a transendothelial migration signature using information from the Gene-Set Enrichment Analysis (GSEA) Molecular Signature Database (MSigDB) and the Ingenuity database (listed in Table S7). Superimposition of this signature onto a plot comparing the transcriptomes of denervated and innervated hindpaw endothelial cells revealed a significant underrepresentation of these transcripts in the denervated hindpaw (Fig. 4*D*). The genes most differentially expressed (Table S7) include representatives of several signaling pathways critical for regulating vascular permeability (Fig. S2).

Discussion

The major goals of this study were to establish a mouse model for hemiplegia-induced protection from RA and to exploit this model to elucidate the mechanistic underpinnings of this fascinating, but little explored, clinical phenomenon. We turned to the well-studied K/BxN serum-transfer system, which mimics many of the clinical and immunological features of human inflammatory arthritis (22). The impact of denervation on the response to arthritogenic serum by mice was astonishingly parallel to the effect of central or peripheral denervation on subsequent RA development by humans. For example, in both cases, denervation is initially proinflammatory, but a long-lasting anti-inflammatory state eventually sets in (Fig. 1*D* and ref. 23). Because of the simplicity of the serum-transfer system, focused on the arthritis effector phase, and because of its tractability to experimental manipulation, easily adapted for genetic or pharmacologic intervention, we could evaluate candidate systems, pathways, and molecules rapidly. Several of our observations merit further discussion.

First, the surgical procedure, which injures nerve fibers of the motor, SNS, PNS, and sensory systems, resulted in extensive,

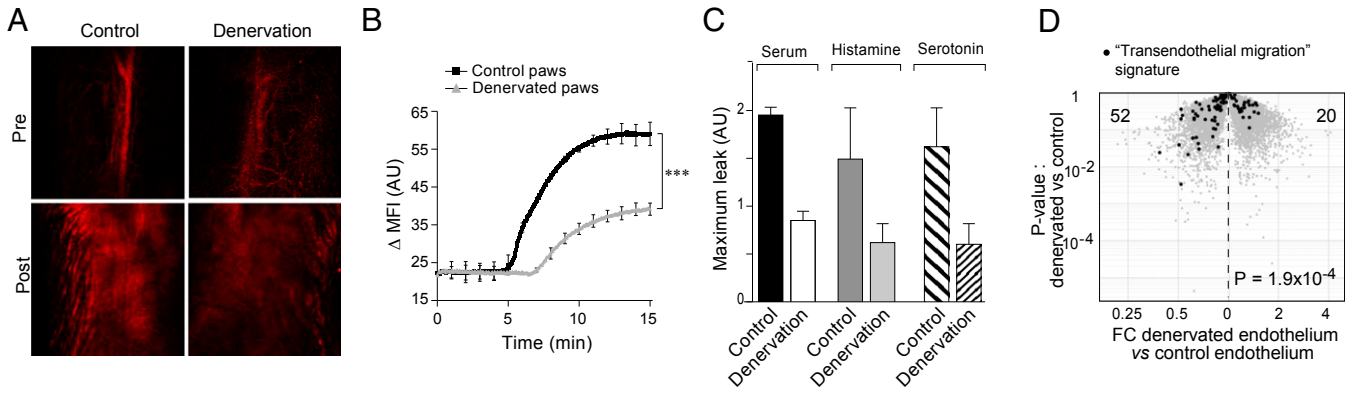

Fig. 4. Effects of hindlimb denervation on the ankle microvasculature. (*A–C*) Inhibition of K/BxN serum-induced vascular leak. The vascular probe AngioSense 680 was i.v. injected 5 min before serum transfer. (*A*) Single-plane confocal micrographs of control and denervated hindpaws just before and 10 min after serum injection. (Magnification: 10×.) (*B*) Quantification of the change in mean fluorescence intensity (ΔMFI) of confocal micrographs obtained every 5 s for 15 min after serum injection. ΔMFI was calculated vis-à-vis the preserum value. Data shown are representative of four mice. ***$P < 0.001$, calculated by the Student *t* test. (*C*) Effect of injecting vasoactive amines instead of serum on vascular leak in innervated vs. denervated hindpaws. $n = 3–4$. (*D*) Changes in endothelial cell transcriptome. Microarray analysis of gene expression by endothelial cells isolated from paws of denervated or sham-operated limbs. Genes from a transendothelial migration signature (Table S7) are highlighted on a volcano plot. *P* value was determined by a χ^2 test.

long-lasting transcriptome changes in the denervated limb, independent of serum transfer. The damage caused by transection of the sciatic and femoral nerves causes what is known as "Wallerian degeneration" (24). Nerve fibers distal to the injury undergo rapid degeneration, with only the sheath remaining to guide regenerative axon sprouting; some retraction of proximal fibers also occurs. At the cellular level, the distal degeneration is dominated by a massive accumulation of macrophages, peaking between days 7 and 14 and then gradually clearing (25). At the molecular level, there is an increase in perineural levels of proinflammatory mediators such as TNF-α, IL-1β, CCL2, and CCL3, even before the expansion of the macrophage population, i.e., at days 1–3 (26, 27). Thus, the denervation-induced transcriptome changes must reflect a complex mix of cellular and molecular responses, of both a degenerative and regenerative nature, as well as more distal effects. Most striking, although not unexpected, was the underrepresentation in the denervated limbs of a group of myelin-related and muscle-associated transcripts and the overrepresentation of transcripts related to tissue regeneration.

Second, we were unable to identify a particular nerve quality required for K/BxN serum-transferred arthritis. This finding contrasts with previous reports of an effect of manipulating the SNS in other mouse models of inflammatory arthritis (sometimes via the same inhibitors) (3, 15). A likely explanation for the divergent results is that the models previously interrogated are rather different: Unlike the K/BxN serum-transfer system, they encompass both the initiation and effector stages of arthritis and depend on the injection of an adjuvant to induce disease. We only can surmise that in the system we used the overall, integrated, quantity or quality of nerve signaling is the critical parameter or, alternatively, that the denervation procedure damaged auxiliary systems.

Third, hindpaw denervation did result in vascular changes known to be detrimental to the progression of arthritis. The K/BxN serum-transferred disease is preceded by and depends on a rapid increase in joint-localized macromolecular permeability of the microvasculature (19, 28). Anti-GPI autoAbs are recognized by FcγRIII, likely on mast cells, which in turn release histamine and serotonin, thereby provoking a transient increase in vascular permeability. Consequently, more anti-GPI autoAbs exit the circulation and deposit in the joints, and more innate immune cells gain access to the periarticular space. Anti-GPI–induced vascular leak was significantly delayed and reduced in denervated hindpaws. Interestingly, unlike the case for control paws, injection of histamine or serotonin into denervated paws did not elicit joint-localized vascular permeability. Because these vasoactive amines bypass the need for anti-GPI, neutrophils, mast cells, and FcγRIII, this result pointed to a possible defect in endothelial cells of the joint.

Indeed, expression of a number of genes implicated in controlling vascular permeability was altered, either negatively or positively, in the endothelium of denervated hindpaws. Among the down-regulated genes whose products promote vessel permeability and cell transmigration are *Axl* and *Jam2*. Axl is a tyrosine kinase crucial in the VEGF-A pathway, downstream of PI3K/AKT activation; *Axl*-null mice showed reduced permeability in several inflammatory contexts (29). Junctional adhesion molecule 2 (encoded by *Jam2*) is an endothelial cell-surface protein that promotes rolling and adhesion of immune cells, a prerequisite for transmigration (30); blockade of this protein abrogated transmigration of primary human peripheral blood leukocytes across umbilical vein endothelial cells (31).

Among the up-regulated genes encoding proteins known to dampen endothelial leak and cellular transmigration are *Argptl4* and *Cry61*. Angiopoietin-like 4, structurally similar to the angiopoietins, protects vascular integrity in contexts of myocardial infarction and tumor metastasis; *Angptl4*-KO mice showed altered VEGFR2/VE-cadherin complexes and disrupted endothelial cell adherens junctions (32, 33). Cysteine-rich angiogenic inducer 61 (encoding by *Cr61*), produced by fibroblasts and endothelial cells, is considered an important matrix protein promoting tissue repair and immune cell adhesion by binding various integrins; high expression of this molecule inhibits transmigration of innate and adaptive immune cells (34). Clearly, transcriptome changes in hindpaw endothelial cells support the notion that vascular alterations in the denervated limbs reduce access to arthritogenic cells and molecules.

Such a scenario makes evolutionary sense. Paralyzed limbs are prone to venous and lymphatic stasis, because of the lack of motor activity, which normally acts as a pump to return blood and lymph centrally to the heart and thoracic duct. Therefore the limb tends to become edematous, increasing the likelihood of microbial infections. Minimizing vascular leak would result in less edema and, thereby, fewer infections.

Materials and Methods

Mice. Male mice (6- to 8-wk-old) of the following strains were purchased from Jackson Laboratory: C57BL/6J, Tie2 reporter (Tg(TIE2GFP)287Sato/J), substance P-deficient (B6.Cg-Tac1tm1Bbm/J), TRPV-deficient (B6.129 × 1-Trpv1tm1Jul/J), and nAchRa7-deficient (B6.129S7-Chrna7tm1Bay/J) mice. All mouse procedures were approved by the institutional subcommittee on research animal care at Massachusetts General Hospital.

Denervation and Arthritis Induction. On the same leg, the sciatic nerve was isolated in the gluteal fossa posteriorly and the femoral nerve was isolated anteriorly distal to the inguinal ligament. Denervation was accomplished by transection and removal of at least 2 mm of nerve. Sham operations were performed on the contralateral leg.

K/BxN serum-transferred arthritis was induced by i.p. injection of 150 μL pooled serum from 8-wk-old K/BxN mice on days 0 and 2. For arthritis reversal, 100 μg of IL-1β was injected i.p. on days 0, 1, and 2. Clinical arthritis was assessed by measuring ankle thickness.

For histological analysis, animals were killed at the indicated time points, and paws were harvested. After decalcification with 9% (vol/vol) formic acid, specimens were processed using standard paraffin embedding and were stained with H&E.

Protease Imaging. Imaging of a fluorescent cathepsin-B–sensitive probe (Prosense; Perkin-Elmer) was performed as described (11). Mice were injected with the probe 9 d after serum treatment and were imaged 1 d later. Images were processed with ImageJ (National Institutes of Health) to define regions of interest and to color-code using Fire filter.

Microarray Analysis. For whole-ankle gene expression, hindpaws of B6 mice were harvested at various time points in the course of disease and prepared as previously described (35). For endothelial cell gene expression, hind paws of Tie2-GFP mice were harvested 10 d after denervation and prepared as above. Cells then were sorted on the GFP signal and directly collected in TRIzol (Life Technologies). All cell populations were generated in triplicate.

RNA was processed and analyzed using M430 2.0 chips (Affymetrix) as detailed previously (35) and updated (36). The analysis of canonical pathways used Ingenuity Pathway Analysis (IPA; Ingenuity Systems). The transendothelial migration signature was generated by extracting gene sets relevant to this function from IPA and MSigDB (www.broad.mit.edu/gsea).

Pharmacological Manipulation. Compounds were diluted in normal saline to the specified concentration and were administered as follows: guanethidine at 0.5 mg daily i.p., 6-OH-dopamine at 80 mg/kg every other day i.p., reserpine at 5 mg/kg every other day i.p., hexamethonium at 5 $mg \cdot kg^{-1} \cdot h^{-1}$ s.c., and mecamylamine at 1 mg/kg daily orally. Administration began on day 0, at the time of serum transfer.

Confocal Imaging of Vessel Permeability. Vascular imaging was performed as previously described (19) after injection of AngioSense 680 (Perkin-Elmer) into serum-transferred or histamine (200 mg/kg)- or serotonin (10 mg/kg)-injected mice. Microscopy was performed with a multichannel upright confocal microscope (Radiance 2100; Bio-Rad Laboratories).

Statistical Analysis. Statistical analysis was performed using the program Prism 5 (GraphPad Software). One-way ANOVA and the Student *t* test were performed as indicated in the figure legends.

ACKNOWLEDGMENTS. This work was funded by National Institutes of Health Grant AI054904 (to D.M., C.B., and R.W.). L.S. was supported by a fellowship from the Deutsche Forschungsgemeinschaft, STA 1025/1-1, and B.A.B. was supported by a Pfizer Postdoctoral Fellowship in Rheumatology/Immunology.

1. Eskandari F, Webster JI, Sternberg EM (2003) Neural immune pathways and their connection to inflammatory diseases. *Arthritis Res Ther* 5(6):251–265.
2. Kass EH, Finland M (1951) The role of adrenal steroids in infection and immunity. *N Engl J Med* 244(13):464–470.
3. Levine JD, Coderre TJ, Helms C, Basbaum AI (1988) Beta 2-adrenergic mechanisms in experimental arthritis. *Proc Natl Acad Sci USA* 85(12):4553–4556.
4. Alawi K, Keeble J (2010) The paradoxical role of the transient receptor potential vanilloid 1 receptor in inflammation. *Pharmacol Ther* 125(2):181–195.
5. Borovikova LV, et al. (2000) Vagus nerve stimulation attenuates the systemic inflammatory response to endotoxin. *Nature* 405(6785):458–462.
6. Coste F, Forestier M (1935) Hemiplegie et nodosities d'Heberden contralaterales. *Bull Mem Soc Med Hop Paris* 51:772–776.
7. Jacqueline F (1953) [A case of evolutive polyarthritis with localisation controlateral to a hemiplegia]. *Rev Rhum Mal Osteoartic* 20(4):323–324.
8. Thompson M, Bywaters EG (1962) Unilateral rheumatoid arthritis following hemiplegia. *Ann Rheum Dis* 21:370–377.
9. Kouskoff V, et al. (1996) Organ-specific disease provoked by systemic autoimmunity. *Cell* 87(5):811–822.
10. Monach PA, Mathis D, Benoist C (2008) The K/BxN arthritis model. *Curr Protoc Immunol* Chapter 15 Unit 15.22.
11. Ji H, et al. (2002) Arthritis critically dependent on innate immune system players. *Immunity* 16(2):157–168.
12. Nigrovic PA, et al. (2007) Mast cells contribute to initiation of autoantibody-mediated arthritis via IL-1. *Proc Natl Acad Sci USA* 104(7):2325–2330.
13. Zhang N, Ahsan MH, Purchio AF, West DB (2005) Serum amyloid A-luciferase transgenic mice: Response to sepsis, acute arthritis, and contact hypersensitivity and the effects of proteasome inhibition. *J Immunol* 174(12):8125–8134.
14. Pongratz G, Straub RH (2013) Role of peripheral nerve fibres in acute and chronic inflammation in arthritis. *Nat Rev Rheumatol* 9(2):117–126.
15. Härle P, Möbius D, Carr DJ, Schölmerich J, Straub RH (2005) An opposing time-dependent immune-modulating effect of the sympathetic nervous system conferred by altering the cytokine profile in the local lymph nodes and spleen of mice with type II collagen-induced arthritis. *Arthritis Rheum* 52(4):1305–1313.
16. Wang H, et al. (2003) Nicotinic acetylcholine receptor alpha7 subunit is an essential regulator of inflammation. *Nature* 421(6921):384–388.
17. Carolan EJ, Casale TB (1993) Effects of neuropeptides on neutrophil migration through noncellular and endothelial barriers. *J Allergy Clin Immunol* 92(4):589–598.
18. Saban MR, Saban R, Bjorling D, Haak-Frendscho M (1997) Involvement of leukotrienes, TNF-alpha, and the LFA-1/ICAM-1 interaction in substance P-induced granulocyte infiltration. *J Leukoc Biol* 61(4):445–451.
19. Binstadt BA, et al. (2006) Particularities of the vasculature can promote the organ specificity of autoimmune attack. *Nat Immunol* 7(3):284–292.
20. Ruiz de Almodovar C, et al. (2011) VEGF mediates commissural axon chemoattraction through its receptor Flk1. *Neuron* 70(5):966–978.
21. Zlokovic BV (2011) Neurovascular pathways to neurodegeneration in Alzheimer's disease and other disorders. *Nat Rev Neurosci* 12(12):723–738.
22. Sachithanandan N, et al. (2011) Macrophage deletion of SOCS1 increases sensitivity to LPS and palmitic acid and results in systemic inflammation and hepatic insulin resistance. *Diabetes* 60(8):2023–2031.
23. Nava P (1953) [Old rheumatoid arthritis; cerebral ictus; acute evolutive outbreak of pain in joints of the hemiplegic side]. *Bras Med* 67(16-17):318–321.
24. Luo L, O'Leary DD (2005) Axon retraction and degeneration in development and disease. *Annu Rev Neurosci* 28:127–156.
25. Mueller M, et al. (2003) Macrophage response to peripheral nerve injury: The quantitative contribution of resident and hematogenous macrophages. *Lab Invest* 83(2):175–185.
26. Perrin FE, Lacroix S, Avilés-Trigueros M, David S (2005) Involvement of monocyte chemoattractant protein-1, macrophage inflammatory protein-1alpha and interleukin-1beta in Wallerian degeneration. *Brain* 128(Pt 4):854–866.
27. Shamash S, Reichert F, Rotshenker S (2002) The cytokine network of Wallerian degeneration: Tumor necrosis factor-alpha, interleukin-1alpha, and interleukin-1beta. *J Neurosci* 22(8):3052–3060.
28. Wipke BT, Wang Z, Kim J, McCarthy TJ, Allen PM (2002) Dynamic visualization of a joint-specific autoimmune response through positron emission tomography. *Nat Immunol* 3(4):366–372.
29. Ruan GX, Kazlauskas A (2012) Axl is essential for VEGF-A-dependent activation of PI3K/Akt. *EMBO J* 31(7):1692–1703.
30. Ludwig RJ, et al. (2005) Junctional adhesion molecules (JAM)-B and -C contribute to leukocyte extravasation to the skin and mediate cutaneous inflammation. *J Invest Dermatol* 125(5):969–976.
31. Johnson-Léger CA, Aurrand-Lions M, Beltraminelli N, Fasel N, Imhof BA (2002) Junctional adhesion molecule-2 (JAM-2) promotes lymphocyte transendothelial migration. *Blood* 100(7):2479–2486.
32. Galaup A, et al. (2006) Angiopoietin-like 4 prevents metastasis through inhibition of vascular permeability and tumor cell motility and invasiveness. *Proc Natl Acad Sci USA* 103(49):18721–18726.
33. Galaup A, et al. (2012) Protection against myocardial infarction and no-reflow through preservation of vascular integrity by angiopoietin-like 4. *Circulation* 125(1):140–149.
34. Löbel M, et al. (2012) CCN1: A novel inflammation-regulated biphasic immune cell migration modulator. *Cell Mol Life Sci* 69(18):3101–3113.
35. Jacobs JP, et al. (2010) Deficiency of CXCR2, but not other chemokine receptors, attenuates autoantibody-mediated arthritis in a murine model. *Arthritis Rheum* 62(7):1921–1932.
36. Burzyn D, et al. (2013) A special population of regulatory T cells potentiates muscle repair. *Cell* 155(6):1282–1295.

Supporting Information

Stangenberg et al. 10.1073/pnas.1410854111

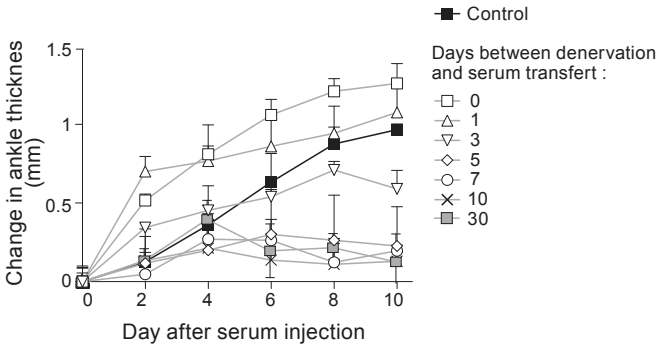

Fig. S1. Impact of time since denervation on protection from K/BxN serum-transferred arthritis. Shown are full curves of ankle thickening over time for the experiment depicted in Fig. 1*D*.

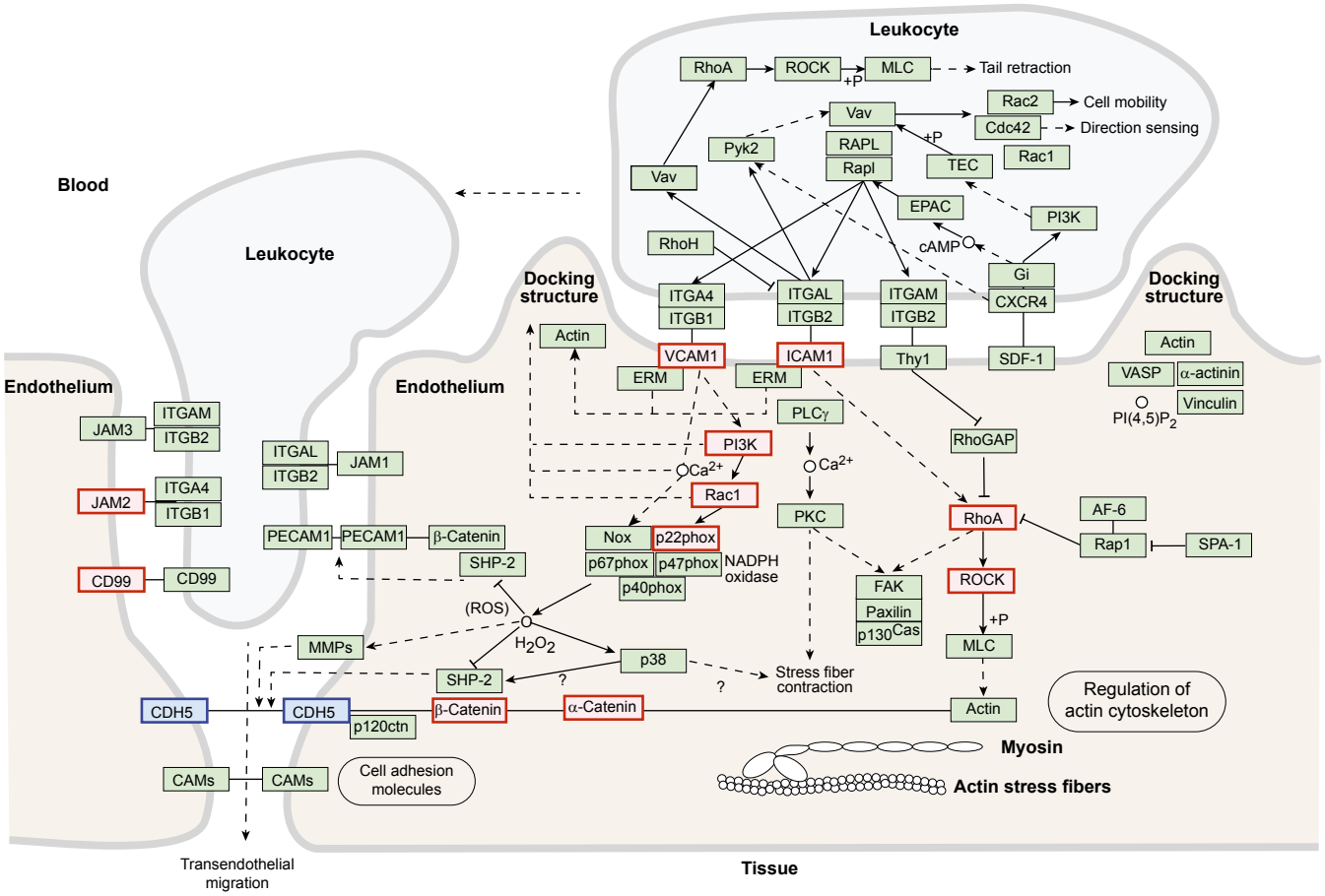

Genes from table S7 corresponding to the highlighted proteins:

- Jam2 (JAM2)
- CD99l2 (CD99 paralog)
- Ctnnb1 (β-catenin)
- Ctnna1 (α-catenin)
- VCAM1
- Icam2 (ICAM1family member)
- Pik3r2 (PI3K regulatory subunit 2 [beta])
- Pik3ca (PI3K catalitic subunit alpha)
- Rac1 (Rac1)
- Cyba (p22phox)
- Rhoa (RhoA)
- Rock1 (ROCK)
- Cdh5 (CDH5)

Fig. S2. Perturbation of the transepithelial migration pathway. Proteins encoded by the down-regulated genes that emerged in Fig. 4*D* and Table S7 are highlighted in red on a map of the transendothelial migration pathway from the Kegg database (www.genome.jp/kegg-bin/show_pathway?hsa04670). CDH5 (blue) is important for endothelial cell–cell contact.

Table S1. Genes most up-regulated in denervated ankles

Probe ID	Gene name	Fold change denervated vs. control	*P* value
1416967_at	*SOX2*	12.9	0.00003
1420992_at	*ANKRD1*	12.8	0.00000
1448169_at	*KRT18*	11.8	0.00010
1449519_at	*GADD45A*	10.9	0.00002
1452968_at	*CTHRC1*	10.2	0.00001
1422606_at	*C1QTNF3*	8.4	0.00010
1420884_at	*SLN*	7.2	0.00026
1435053_s_at	*PLEKHH1*	6.7	0.00002
1436055_at	*LRRC15*	5.4	0.00034
1421698_a_at	*COL19A1*	5	0.00088
1455679_at	*NABP1*	4.9	0.00050
1422562_at	*RRAD*	4.8	0.00169
1424245_at	*Ces2b/Ces2c*	4.7	0.00002
1440878_at	*RUNX1*	4.7	0.00001
1454830_at	*FBN2*	4.5	0.00017
1418726_a_at	*TNNT2*	4.4	0.00061
1452679_at	*TUBB2B*	4.3	0.00042
1431869_at	*5730419F03Rik*	4.1	0.00191
1419684_at	*Ccl8*	4.1	0.00069
1419391_at	*MYOG*	3.9	0.00005
1451287_s_at	*AIF1L*	3.8	0.00130
1451191_at	*CRABP2*	3.8	0.00014
1439768_x_at	*SEMA4F*	3.8	0.00015
1423691_x_at	*KRT8*	3.7	0.00031
1442140_at	*TNN*	3.7	0.00005
1438540_at	*COL25A1*	3.6	0.00269
1427910_at	*CST6*	3.6	0.00049
1448194_a_at	*H19*	3.6	0.00282
1416572_at	*MMP14*	3.6	0.03154
1448201_at	*SFRP2*	3.6	0.00079
1424831_at	*CPNE2*	3.4	0.00120
1448901_at	*CPXM1*	3.4	0.00116
1422580_at	*MYL4*	3.4	0.00086
1419060_at	*GZMB*	3.3	0.00150
1418945_at	*MMP3*	3.3	0.00140
1418547_at	*TFPI2*	3.2	0.00080
1447890_at	*RCN1*	3.1	0.00852
1434291_a_at	*SERF1A/SERF1B*	3.1	0.00556
1449532_at	*CHRNG*	3	0.00110
1440085_at	*EDA2R*	3	0.00047
1449378_at	*KRT27*	3	0.01881
1439204_at	*SCN3A*	3	0.00483
1422629_s_at	*SHROOM3*	3	0.00259
1460227_at	*TIMP1*	3	0.00043
1422514_at	*AEBP1*	2.9	0.00477
1422573_at	*AMPD3*	2.9	0.00062
1417231_at	*CLDN2*	2.9	0.00037
1430353_at	*GLIS3*	2.9	0.00123
1435354_at	*KCNJ15*	2.9	0.00025
1450013_at	*MYL12A*	2.9	0.00067
1434709_at	*NRCAM*	2.9	0.00012
1446951_at	*P4HA3*	2.9	0.00218
1420731_a_at	*CSRP2*	2.8	0.00053
1433474_at	*EDIL3*	2.8	0.01032
1416021_a_at	*FABP5*	2.8	0.00402
1424882_a_at	*Nt5dc2*	2.8	0.00245
1423606_at	*POSTN*	2.8	0.00221
1455203_at	*A930003A15Rik*	2.7	0.00047
1427168_a_at	*COL14A1*	2.7	0.00055
1452957_at	*KRTAP3-2*	2.7	0.00499
1437152_at	*MEX3B*	2.7	0.00851

Table S1. Cont.

Probe ID	Gene name	Fold change denervated vs. control	*P* value
1421977_at	*MMP19*	2.7	0.00536
1421172_at	*ADAM12*	2.6	0.00219
1424638_at	*CDKN1A*	2.6	0.00024
1418852_at	*CHRNA1*	2.6	0.00068
1460259_s_at	*Clca1/Clca2*	2.6	0.05195
1450567_a_at	*COL2A1*	2.6	0.12706
1416740_at	*COL5A1*	2.6	0.00086
1438883_at	*FGF5*	2.6	0.00013
1419150_at	*MYF6*	2.6	0.00150
1460187_at	*SFRP1*	2.6	0.03081
1416065_a_at	*ANKRD10*	2.5	0.00034
1426955_at	*COL18A1*	2.5	0.00123
1436659_at	*DCLK1*	2.5	0.00015
1416514_a_at	*FSCN1*	2.5	0.00035
1452947_at	*GPRC5C*	2.5	0.00283
1438532_at	*HMCN1*	2.5	0.00368
1416028_a_at	*HN1*	2.5	0.00085
1417359_at	*MFAP2*	2.5	0.00105
1424010_at	*MFAP4*	2.5	0.01103
1448254_at	*PTN*	2.5	0.00210
1428983_at	*SCXA/SCXB*	2.5	0.00084
1455224_at	*ANGPTL1*	2.4	0.00351
1434411_at	*COL12A1*	2.4	0.00092
1450625_at	*COL5A2*	2.4	0.00251
1421074_at	*CYP7B1*	2.4	0.00121
1427537_at	*EPPK1*	2.4	0.11406
1454674_at	*FEZ1*	2.4	0.00066
1452799_at	*FGGY*	2.4	0.00005
1419139_at	*GDF5*	2.4	0.00135
1444599_at	*HERC4*	2.4	0.01578
1430062_at	*HHIPL1*	2.4	0.00125
1436223_at	*ITGB8*	2.4	0.00039
1449963_at	*Krtap9-3*	2.4	0.00437
1420741_x_at	*Lce1i*	2.4	0.14935
1416136_at	*MMP2*	2.4	0.00213
1428942_at	*MT1H*	2.4	0.00262
1450437_a_at	*NCAM1*	2.4	0.01603
1454903_at	*NGFR*	2.4	0.00187
1455034_at	*NR4A2*	2.4	0.00237
1423905_at	*Pvr*	2.4	0.00074
1437231_at	*SLITRK6*	2.4	0.00139
1428386_at	*ACSL3*	2.3	0.00103
1419621_at	*ANKRD2*	2.3	0.00462
1444564_at	*APOD*	2.3	0.01541
1434513_at	*ATP13A3*	2.3	0.00063
1433434_at	*AW551984*	2.3	0.00056
1435286_at	*EPHA5*	2.3	0.00079
1460412_at	*FBLN7*	2.3	0.00996
1418420_at	*MYOD1*	2.3	0.00083
1419309_at	*PDPN*	2.3	0.00023
1453839_a_at	*PI16*	2.3	0.01409
1416211_a_at	*PTN*	2.3	0.01739
1424507_at	*RIN1*	2.3	0.00041
1460129_at	*SLC6A2*	2.3	0.00334
1420833_at	*VAMP2*	2.3	0.00809
1442063_at	*ADAMTSL1*	2.2	0.00159
1421344_a_at	*AJUBA*	2.2	0.02446
1422789_at	*ALDH1A2*	2.2	0.00127
1427457_a_at	*BMP1*	2.2	0.01077
1427986_a_at	*COL16A1*	2.2	0.00050

Table S1. Cont.

Probe ID	Gene name	Fold change denervated vs. control	*P* value
1427884_at	*COL3A1*	2.2	0.00041
1426947_x_at	*COL6A2*	2.2	0.00106
1452366_at	*CSGALNACT1*	2.2	0.00007
1455872_at	*FAM167A*	2.2	0.00115
1419080_at	*GDNF*	2.2	0.00475
1422293_a_at	*KCTD1*	2.2	0.00017
1429987_at	*KIAA1199*	2.2	0.02874
1453523_at	*KRTAP17-1*	2.2	0.00321
1451774_at	*KRTAP4-3*	2.2	0.02620
1437109_s_at	*LSM6*	2.2	0.00193
1417281_a_at	*MMP23B*	2.2	0.00026
1416149_at	*OLIG1*	2.2	0.00439
1458813_at	*SCN5A*	2.2	0.00204
1433571_at	*SERINC5*	2.2	0.00006
1427035_at	*SLC39A14*	2.2	0.00046
1419588_at	*SPAG1*	2.2	0.00666
1423135_at	*THY1*	2.2	0.00990
1428074_at	*TMEM158*	2.2	0.00087
1442590_at	*Tnfrsf22/Tnfrsf23*	2.2	0.00013
1448501_at	*TSPAN6*	2.2	0.00051
1416431_at	*TUBB6*	2.2	0.00074
1430596_s_at	*VGLL3*	2.2	0.02350
1431554_a_at	*ANXA9*	2.1	0.09248
1431856_a_at	*C1qtnf6*	2.1	0.00184
1439327_at	*CCBE1*	2.1	0.02058
1460125_at	*CCDC141*	2.1	0.01306
1419703_at	*COL5A3*	2.1	0.00201
1424131_at	*COL6A3*	2.1	0.00032
1417312_at	*DKK3*	2.1	0.00102
1427298_at	*Dnm3os*	2.1	0.00504
1449204_at	*GJB5*	2.1	0.10052
1456242_at	*Gm7325*	2.1	0.02783
1454693_at	*HDAC4*	2.1	0.00124
1417014_at	*HSPB8*	2.1	0.01607
1416473_a_at	*IGDCC4*	2.1	0.00660
1427164_at	*IL13RA1*	2.1	0.01206
1441307_at	*KRTAP4-12*	2.1	0.01656
1424114_s_at	*LAMB1*	2.1	0.00045
1417942_at	*LYPD3*	2.1	0.10545
1416006_at	*MDK*	2.1	0.00536
1436713_s_at	*Meg3*	2.1	0.03829
1417234_at	*MMP11*	2.1	0.04670
1417256_at	*MMP13*	2.1	0.03198
1439364_a_at	*MMP2*	2.1	0.00160
1423172_at	*NAPB*	2.1	0.00154
1453840_at	*PABPC1*	2.1	0.09662
1435644_at	*SH3PXD2B*	2.1	0.00139
1455149_at	*SH3RF1*	2.1	0.00525
1433575_at	*SOX4*	2.1	0.00180
1427919_at	*SRPX2*	2.1	0.00080
1434442_at	*STBD1*	2.1	0.00070
1416783_at	*TAC1*	2.1	0.01073
1416342_at	*TNC*	2.1	0.01088
1418572_x_at	*TNFRSF12A*	2.1	0.02373
1423312_at	*TPBG*	2.1	0.00656
1421424_a_at	*ANPEP*	2	0.00069
1417225_at	*ARL6IP5*	2	0.00562
1419028_at	*ARPP21*	2	0.00029
1427508_at	*ARSI*	2	0.00011

Table S1. Cont.

Probe ID	Gene name	Fold change denervated vs. control	*P* value
1437092_at	*CLIP4*	2	0.00515
1448316_at	*CMTM3*	2	0.00178
1448694_at	*JUN*	2	0.00023
1430669_at	*KRTAP4-11*	2	0.05549
1427211_at	*KRTAP8-1*	2	0.00482
1447830_s_at	*RGS2*	2	0.00634
1436684_a_at	*RIOK2*	2	0.00202
1423428_at	*ROR2*	2	0.01045
1423310_at	*TPBG*	2	0.01057

Table S2. Genes most down-regulated in denervated ankles

Probe ID	Gene name	Fold change denervated vs. control	*P* value
1433532_a_at	*MBP*	0.054	0.00002
1444504_at	*DHRS7C*	0.070	0.00014
1448394_at	*MYL2*	0.095	0.00060
1423253_at	*MPZ*	0.098	0.00004
1418589_a_at	*MLF1*	0.101	0.00001
1434449_at	*AQP4*	0.115	0.00039
1450940_at	*GDAP1*	0.127	0.00001
1422798_at	*CNTNAP2*	0.136	0.00007
1449398_at	*RPL3L*	0.139	0.00040
1432001_at	*MSS51*	0.150	0.00015
1417275_at	*MAL*	0.160	0.00023
1417889_at	*APOBEC2*	0.178	0.00076
1448636_at	*MYOZ1*	0.181	0.00001
1452474_a_at	*ART3*	0.198	0.00003
1438641_x_at	*FAM57B*	0.199	0.00768
1424553_at	*HHATL*	0.199	0.00110
1451322_at	*CMBL*	0.200	0.00013
1428014_at	*Hist2h4* (includes others)	0.209	0.00719
1428722_at	*CKMT2*	0.215	0.00015
1434008_at	*SCN4B*	0.218	0.00137
1430738_at	*MYOZ3*	0.219	0.00009
1419063_at	*UGT8*	0.220	0.00017
1415927_at	*ACTC1*	0.231	0.00642
1425164_a_at	*PHKG1*	0.232	0.00015
1440435_at	*KY*	0.234	0.00099
1438676_at	*Gbp6* (includes others)	0.237	0.00015
1429598_at	*2310042D19Rik*	0.238	0.00070
1420858_at	*PKIA*	0.239	0.00505
1449547_at	*ASB14*	0.240	0.00005
1417673_at	*GRB14*	0.242	0.00015
1416835_s_at	*AMD1*	0.244	0.00110
1443855_at	*KCNC1*	0.248	0.00429
1418709_at	*COX7A1*	0.249	0.00210
1441111_at	*MYLK4*	0.250	0.00066
1444643_at	*CKM*	0.259	0.00057
1434722_at	*AMPD1*	0.261	0.00000
1439491_at	*LRRC38*	0.261	0.00084
1417807_at	*UFSP1*	0.264	0.00490
1422153_a_at	*ASB11*	0.265	0.00116
1441305_at	*NEDD4L*	0.272	0.00241
1435743_at	*KLHL23/PHOSPHO2-KLHL23*	0.273	0.00004
1457311_at	*CAMK2A*	0.274	0.00376
1437030_at	*PLCD4*	0.276	0.00021
1418951_at	*TXLNB*	0.276	0.00003
1419145_at	*SMTNL1*	0.277	0.00103
1445841_at	*LRRC39*	0.277	0.00086
1453657_at	*2310065F04Rik*	0.281	0.00031
1423084_at	*B3GALT2*	0.293	0.00006
1417481_at	*RAMP1*	0.296	0.00051
1434542_at	*GPT2*	0.297	0.00039
1424531_a_at	*TCEA3*	0.298	0.00092
1422644_at	*SH3BGR*	0.304	0.00026
1456819_at	*NRN1L*	0.308	0.00259
1422500_at	*IDH3A*	0.308	0.00001
1449079_s_at	*ST3GAL6*	0.310	0.00031
1418328_at	*CPT1B*	0.310	0.00901
1421690_s_at	*AGRP*	0.312	0.00015
1448602_at	*PYGM*	0.313	0.00011
1458587_at	*2310047D07Rik*	0.314	0.00290
1420346_at	*ASB12*	0.315	0.00120
1448530_at	*GMPR*	0.317	0.00051

Table S2. Cont.

Probe ID	Gene name	Fold change denervated vs. control	*P* value
1434766_at	*PRKAA2*	0.323	0.00099
1418395_at	*SLC47A1*	0.324	0.00103
1422635_at	*ACHE*	0.326	0.00149
1424268_at	*SMOX*	0.329	0.00306
1429419_at	*RIIAD1*	0.331	0.00438
1455842_x_at	*USP15*	0.331	0.00040
1436440_at	*SLC25A12*	0.332	0.00003
1432420_a_at	*2310002L09Rik*	0.333	0.00075
1416034_at	*Cd24a*	0.334	0.00014
1434738_at	*TARSL2*	0.335	0.00002
1428025_s_at	*PITPNC1*	0.336	0.01136
1458193_at	*PMP2*	0.339	0.00021
1457031_at	*FSD2*	0.341	0.00022
1424649_a_at	*TSPAN8*	0.341	0.00563
1427556_at	*MYLK2*	0.342	0.06953
1439627_at	*ZIC1*	0.348	0.00091
1417951_at	*ENO3*	0.350	0.00444
1451801_at	*TRDN*	0.350	0.00007
1429083_at	*AGL*	0.350	0.00383
1419700_a_at	*PROM1*	0.352	0.00024
1418117_at	*NDUFS4*	0.352	0.00032
1449005_at	*SLC16A3*	0.354	0.00286
1429918_at	*ARHGAP20*	0.357	0.00348
1422795_at	*CUL3*	0.358	0.00629
1449818_at	*ABCB4*	0.358	0.00014
1427527_a_at	*PTHLH*	0.359	0.00190
1449893_a_at	*LRIG1*	0.359	0.00088
1417042_at	*SLC37A4*	0.361	0.00028
1423422_at	*ASB4*	0.362	0.00053
1457323_at	*SMCO3*	0.363	0.00007
1448607_at	*NAMPT*	0.364	0.01493
1419518_at	*TUBA8*	0.364	0.00429
1419301_at	*FZD4*	0.366	0.00020
1428444_at	*ASB2*	0.368	0.00391
1431714_at	*2310015D24Rik*	0.369	0.00003
1449383_at	*ADSSL1*	0.371	0.00054
1427768_s_at	*MYL3*	0.372	0.04081
1428991_at	*HRASLS*	0.372	0.00004
1452985_at	*UACA*	0.373	0.00041
1450203_at	*SMYD1*	0.375	0.01279
1435659_a_at	*TPI1*	0.376	0.00003
1448628_at	*SCG3*	0.376	0.00024
1418181_at	*PTP4A3*	0.376	0.00428
1456468_x_at	*MYADML2*	0.377	0.00031
1437637_at	*PHTF2*	0.380	0.01127
1423852_at	*SHISA2*	0.381	0.00018
1447934_at	*C12orf5*	0.382	0.00959
1458368_at	*MYH4*	0.383	0.03824
1421063_s_at	*SNURF*	0.384	0.00994
1427213_at	*PFKFB1*	0.385	0.00050
1438720_at	*KIAA0408*	0.388	0.00018
1417279_at	*ITPR1*	0.388	0.00035
1423183_at	*LGI1*	0.391	0.00126
1425710_a_at	*HOMER1*	0.392	0.03643
1457275_at	*SYNM*	0.392	0.02330
1426180_a_at	*Smr2*	0.394	0.00040
1434100_x_at	*PPARGC1A*	0.396	0.00181
1422033_a_at	*CNTF*	0.397	0.00209
1420805_at	*MYL10*	0.398	0.00961
1443575_at	*2310040G24Rik*	0.401	0.00128
1454867_at	*MN1*	0.401	0.00066

Table S2. Cont.

Probe ID	Gene name	Fold change denervated vs. control	*P* value
1438012_at	*PPM1L*	0.402	0.00286
1422184_a_at	*AK1*	0.403	0.00174
1421413_a_at	*PDLIM5*	0.404	0.00390
1438175_x_at	*MYOM2*	0.404	0.04771
1455182_at	*KIF1B*	0.404	0.00516
1449078_at	*ST3GAL6*	0.405	0.00007
1452465_at	*MYH1*	0.405	0.00047
1442769_at	*MYBPC1*	0.406	0.00135
1433590_at	*HERC3*	0.407	0.00009
1422195_s_at	*TBX15*	0.410	0.00228
1424362_at	*PPAPDC3*	0.411	0.00976
1415958_at	*SLC2A4*	0.413	0.00661
1436501_at	*MTUS1*	0.413	0.00004
1427582_at	*FGF6*	0.414	0.00147
1448300_at	*MGST3*	0.415	0.00887
1450970_at	*GOT1*	0.415	0.00036
1423285_at	*COCH*	0.417	0.00707
1422744_at	*PHKA1*	0.417	0.00256
1433720_s_at	*CHCHD10*	0.417	0.02714
1416432_at	*PFKFB3*	0.418	0.00002
1424393_s_at	*ADHFE1*	0.419	0.00083
1451149_at	*PGM1*	0.419	0.00021
1418252_at	*PADI2*	0.420	0.00072
1434499_a_at	*LDHB*	0.420	0.00440
1424838_at	*NCMAP*	0.421	0.00506
1425518_at	*RAPGEF4*	0.421	0.00569
1436332_at	*HSPB6*	0.423	0.00146
1456793_at	*CYTL1*	0.423	0.00769
1427157_at	*CCDC85A*	0.423	0.00129
1428323_at	*GPD2*	0.424	0.00097
1422927_at	*YIPF7*	0.425	0.00072
1425644_at	*LEPR*	0.425	0.02415
1453003_at	*SORL1*	0.425	0.00017
1440962_at	*SLC8A3*	0.426	0.00095
1438201_at	*PDP1*	0.426	0.00778
1451811_at	*CACNG6*	0.427	0.00132
1423238_at	*ITGB1BP2*	0.427	0.00100
1427591_at	*CLCN1*	0.428	0.00562
1416007_at	*SATB1*	0.430	0.00067
1418311_at	*FN3K*	0.431	0.01182
1428557_a_at	*OSGEPL1*	0.432	0.00059
1454720_at	*HS3ST5*	0.432	0.00288
1450130_at	*XPR1*	0.433	0.00110
1439019_at	*FRAS1*	0.434	0.00041
1450725_s_at	*CA14*	0.435	0.00342
1417877_at	*EEPD1*	0.435	0.00001
1429071_at	*ME3*	0.435	0.00149
1419056_at	*RTN2*	0.435	0.00701
1452879_at	*SYNPO2*	0.436	0.00062
1451707_s_at	*SLC41A3*	0.436	0.01260
1444341_at	*MYBPC1*	0.439	0.05423
1456838_at	*LINGO3*	0.440	0.01879
1422253_at	*COL10A1*	0.441	0.01314
1451440_at	*CHODL*	0.445	0.00094
1424631_a_at	*Ighg*	0.446	0.05460
1455267_at	*ESRRG*	0.447	0.00536
1418952_at	*TXLNB*	0.447	0.00040
1434647_at	*EGFLAM*	0.448	0.00724
1448826_at	*MYH6*	0.448	0.02452
1439505_at	*CLIC5*	0.450	0.00193
1441384_at	*GADL1*	0.451	0.01458

Table S2. Cont.

Probe ID	Gene name	Fold change denervated vs. control	*P* value
1419109_at	*HRC*	0.451	0.00717
1436411_at	*ATP13A5*	0.453	0.00432
1424563_at	*SLC25A4*	0.454	0.00075
1423150_at	*Scg5*	0.455	0.00003
1433628_at	*COQ10A*	0.455	0.00194
1450017_at	*CCNG1*	0.456	0.00436
1425861_x_at	*CACNA2D1*	0.456	0.10192
1431083_a_at	*1810014B01Rik*	0.457	0.00411
1452678_a_at	*CCBL1*	0.458	0.00265
1448147_at	*TNFRSF19*	0.458	0.00417
1422692_at	*SUB1*	0.459	0.00077
1450490_at	*KCNA7*	0.461	0.00601
1423136_at	*FGF1*	0.462	0.00010
1455909_at	*Spink11/Spinkl*	0.462	0.02169
1427427_at	*RYR3*	0.463	0.00005
1433691_at	*PPP1R3C*	0.463	0.00146
1449088_at	*FBP2*	0.464	0.00369
1426043_a_at	*CAPN3*	0.464	0.00094
1451156_s_at	*VLDLR*	0.464	0.00176
1460434_at	*FUNDC2*	0.465	0.00159
1425792_a_at	*RORC*	0.465	0.00099
1419748_at	*ABCD2*	0.466	0.01499
1418373_at	*PGAM2*	0.467	0.00211
1455473_at	*USP13*	0.467	0.00076
1451751_at	*DDIT4L*	0.467	0.01385
1460500_at	*Gm3715*	0.468	0.06068
1452661_at	*TFRC*	0.468	0.00100
1441581_at	*Asb10*	0.468	0.00697
1439669_at	*C3orf18*	0.470	0.00975
1430176_at	*KBTBD13*	0.470	0.00019
1426460_a_at	*UGP2*	0.470	0.00083
1434553_at	*TMEM56*	0.470	0.00096
1418282_x_at	*SERPINA1*	0.470	0.06118
1449218_at	*Cox8b*	0.471	0.01099
1419090_x_at	*KLK3*	0.472	0.00669
1455234_at	*B3GALT1*	0.473	0.00167
1437197_at	*SORBS2*	0.475	0.00054
1455277_at	*HHIP*	0.476	0.01704
1458635_at	*Mettl21e*	0.477	0.00099
1425275_at	*ASPH*	0.477	0.00066
1428163_at	*SAR1B*	0.478	0.00002
1444789_at	*1700120C14Rik*	0.480	0.01104
1429552_at	*WDR16*	0.480	0.01738
1422871_at	*KCNJ12*	0.482	0.01056
1417542_at	*RPS6KA2*	0.482	0.00077
1439848_at	*BVES*	0.483	0.00042
1422852_at	*CIB2*	0.483	0.00993
1458425_at	*A430046D13Rik*	0.484	0.00933
1437302_at	*ADRB2*	0.485	0.00045
1442339_at	*Stfa2/Stfa2l1*	0.485	0.02084
1418210_at	*Pfn2*	0.485	0.00000
1452005_at	*DLAT*	0.486	0.00458
1418370_at	*TNNC1*	0.487	0.00136
1457227_at	*Gm11266*	0.487	0.00119
1423583_at	*FEM1A*	0.488	0.00048
1456386_at	*RBM39*	0.488	0.05098
1436279_at	*SLC26A7*	0.488	0.10083
1424062_at	*UBE2D1*	0.488	0.00010
1438608_at	*TNNI2*	0.489	0.00720
1450505_a_at	*FAM134B*	0.489	0.02956
1425143_a_at	*NDUFS1*	0.490	0.00060

Table S2. Cont.

Probe ID	Gene name	Fold change denervated vs. control	*P* value
1420654_a_at	*GBE1*	0.491	0.00051
1434196_at	*DNAJA4*	0.491	0.00022
1437259_at	*SLC9A2*	0.492	0.00167
1416468_at	*ALDH1A1*	0.492	0.00181
1436889_at	*GABRA1*	0.493	0.00068
1460426_at	*PDE4DIP*	0.494	0.01458
1448136_at	*ENPP2*	0.494	0.00731
1434572_at	*Hdac9*	0.494	0.01315
1416752_at	*Ldb3*	0.494	0.00293
1451650_at	*DDO*	0.495	0.00279
1427915_s_at	*TCEB1*	0.497	0.00086
1426850_a_at	*MAP2K6*	0.498	0.00478
1451152_a_at	*ATP1B1*	0.498	0.00012
1418155_at	*MYOT*	0.499	0.00017

Genes highlighted in blue are muscle homeostasis/function genes (1).

1. Burzyn D, et al. (2013) A special population of regulatory T cells potentiates muscle repair. *Cell* 155(6):1282–1295.

Table S3. Pathways enriched in up-regulated genes in denervated ankles

Canonical pathway	-log (*P* value)	Molecules up-regulated in denervated ankle
Inhibition of matrix metalloproteases	11.50	MMP23B,ADAM12,MMP3,TIMP1,MMP14, MMP13,MMP2,MMP11,TFPI2,MMP19
Bladder cancer signaling	6.35	MMP23B,MMP3,MMP14,CDKN1A,MMP13, MMP2,MMP11,MMP19,FGF5
Granulocyte adhesion and diapedesis	5.89	MMP23B,MMP3,Ccl8,MMP14,NGFR,MMP13,THY1, MMP2,MMP11,CLDN2,MMP19
Leukocyte extravasation signaling	4.96	MMP23B,EDIL3,MMP3,TIMP1,MMP14,MMP13,THY1, MMP2,MMP11,CLDN2,MMP19
HIF1α signaling	4.86	MMP23B,JUN,MMP3,MMP14,MMP13,MMP2,MMP11,MMP19
Agranulocyte adhesion and diapedesis	4.80	MMP23B,MMP3,Ccl8,MMP14,MYL4,MMP13,MMP2,MMP11, CLDN2,MMP19
Atherosclerosis signaling	4.32	COL5A3,MMP3,COL2A1,MMP13,COL18A1,COL3A1,TNFRSF12A, APOD
Intrinsic prothrombin activation pathway	3.56	COL5A3,COL2A1,COL18A1,COL3A1
Role of osteoblasts, osteoclasts and chondrocytes in rheumatoid arthritis	3.01	SFRP2,JUN,MMP3,DKK3,MMP14,NGFR,MMP13,SFRP1,BMP1
Axonal guidance signaling	2.44	MYL12A,TUBB6,ADAM12,NGFR,EPHA5,MYL4,MMP13,SEMA4F, MMP2,MMP11,TUBB2B,BMP1
Hepatic fibrosis/hepatic stellate cell activation	2.28	TIMP1,NGFR,MYL4,MMP13,MMP2,COL3A1
Colorectal cancer metastasis signaling	2.26	MMP23B,JUN,MMP3,MMP14,MMP13,MMP2,MMP11,MMP19
Dendritic cell maturation	2.08	COL5A3,NGFR,FSCN1,COL2A1,COL18A1,COL3A1
Oxidative ethanol degradation III	1.87	ACSL3,ALDH1A2
Wnt/β-catenin signaling	1.87	SOX2,SOX4,SFRP2,JUN,DKK3,SFRP1
Ethanol degradation IV	1.77	ACSL3,ALDH1A2
Role of macrophages, fibroblasts and endothelial cells in rheumatoid arthritis	1.73	ROR2,SFRP2,JUN,MMP3,DKK3,NGFR,MMP13,SFRP1

Table S4. Pathways enriched in down-regulated genes in denervated ankles

Canonical pathway	-log (*P* value)	Molecules
Calcium signaling	7.52	MYH4,MYH6,TNNI2,MYL2,TNNC1,TRDN,SLC8A3,ITPR1,Hdac9,CAMK2A,RYR3, ASPH,ACTC1,MYL3,MYH1
Cellular effects of sildenafil (Viagra)	4.90	MYH4,CACNG6,MYH6,MYL10,MYL2,ITPR1,ACTC1,PLCD4,MYL3,MYH1
Glycogen degradation II	3.74	PYGM,PGM1,AGL
Glycolysis I	3.51	TPI1,ENO3,PGAM2,FBP2
Gluconeogenesis I	3.51	ENO3,ME3,PGAM2,FBP2
Glycogen degradation III	3.41	PYGM,PGM1,AGL
AMPK signaling	3.21	PFKFB3,AK1,CKM,PFKFB1,CPT1B,PPM1L,PRKAA2,ADRB2
Actin cytoskeleton signaling	2.94	MYH4,MYH6,MYL10,MYL2,MYLK2,ACTC1,MYL3,FGF6,FGF1,MYH1
Creatine-phosphate biosynthesis	2.87	CKMT2,CKM
Epithelial adherens junction signaling	2.87	MYH4,MYH6,TUBA8,MYL2,ACTC1,MYL3,FGF1,MYH1
Glycogen biosynthesis II (from UDP-D-glucose)	2.65	UGP2,GBE1
Protein kinase A SIGNALING	2.54	MYH4,CAMK2A,PYGM,MYL10,MYL2,TNNI2,PPP1R3C,RYR3,MYLK2,ITPR1, PLCD4,MYL3,PHKG1
Xenobiotic metabolism signaling	2.53	CUL3,MAP2K6,ALDH1A1,CAMK2A,PPM1L,UGT8,SMOX,HS3ST5,MGST3,PPARGC1A
Hepatic fibrosis/hepatic stellate cell activation	2.37	MYH4,MYH6,MYL2,LEPR,MYL3,FGF1,MYH1
ILK signaling	2.31	MAP2K6,MYH4,MYH6,MYL2,PPM1L,ACTC1,MYL3,MYH1
Tight junction signaling	2.19	MYH4,MYH6,MYL2,PPM1L,ACTC1,MYL3,MYH1
Noradrenaline and adrenaline degradation	2.11	ALDH1A1,SMOX,ADHFE1

Table S5. Genes up-regulated in denervated ankles on day 4 after serum transfer

Probe ID	Gene name	Fold change denervated vs. control	*P* value
1453214_at	*LRRC15*	5.843081	2.85E-04
AFFX-18SRNAMur/X00686_5_at	*Rn18s*	3.088555	0.009669
1417860_a_at	*SPON2*	2.876554	0.008406
1422831_at	*FBN2*	2.755031	0.002243
1431609_a_at	*ACP5*	2.615229	0.009661
1448669_at	*DKK3*	2.459039	8.20E-04
1416298_at	*MMP9*	2.457137	0.0094
1421689_at	*Krtap19-5*	2.436943	2.98E-04
1418063_at	*KERA*	2.423395	0.011763
1452365_at	*CSGALNACT1*	2.415315	6.29E-05
1424113_at	*LAMB1*	2.348265	1.30E-04
1455965_at	*ADAMTS4*	2.33525	0.014686
1424271_at	*DCLK1*	2.330379	0.002748
1444176_at	*ATP6V0D2*	2.327169	0.005595
1450652_at	*CTSK*	2.22709	0.004265
1419156_at	*SOX4*	2.181983	5.13E-04
1417851_at	*CXCL13*	2.173845	0.003969
1438403_s_at	*MALAT1*	2.154024	0.009691
1422640_at	*Pcdhb9*	2.151252	0.005643
1430584_s_at	*CA3*	2.125199	0.022839
1437218_at	*FN1*	2.114524	0.011323
1437057_at	*MEGF6*	2.113564	1.23E-04
1424902_at	*PLXDC1*	2.108408	0.010111
1419276_at	*ENPP1*	2.102984	0.003997
1451446_at	*ANTXR1*	2.0689	1.78E-04
1442115_at	*PIEZO2*	2.06038	0.00265
1428834_at	*DUSP4*	2.048597	0.008967
1438020_at	*HAPLN1*	2.044728	0.003845
1422148_at	*MATN3*	2.023393	1.12E-04
1454995_at	*DDAH1*	2.020484	0.001656
1439078_at	*KLHL4*	2.017414	0.011682
1454877_at	*SERTAD4*	2.014855	0.002512
1424762_at	*C1QTNF5*	2.008849	0.004604

Table S6. Genes down-regulated in denervated ankles on day 4 after serum transfer

Probe ID	Gene name	Fold change denervated vs. control	*P* value
1450828_at	*SYNPO2*	0.318	0.0001
1453141_at	*0610009L18Rik*	0.325	0.0038
1429700_at	*3110040M04Rik*	0.331	0.0023
1439096_at	*DDO*	0.384	0.0018
1429621_at	*CAND2*	0.397	0.0007
1450788_at	*SAA1*	0.397	0.0261
1451488_at	*FITM1*	0.406	0.0011
1418412_at	*TPD52L1*	0.418	0.0049
1417050_at	*C1QTNF4*	0.421	0.0060
1451635_at	*SLC22A9*	0.424	0.0029
1458455_at	*ABRA*	0.424	0.0353
1449969_at	*TMOD4*	0.438	0.0008
1429888_a_at	*HSPB2*	0.440	0.0010
1450449_a_at	*RILPL1*	0.441	0.0017
1432579_at	*RSPH3*	0.443	0.0177
1429260_at	*1810014B01Rik*	0.444	0.0025
1434756_at	*5430421B17*	0.444	0.0006
1421254_a_at	*SGCG*	0.446	0.0014
1430522_a_at	*VAMP5*	0.446	0.0080
1451372_a_at	*ART1*	0.447	0.0019
1449340_at	*SOSTDC1*	0.449	0.0013
1457633_x_at	*COX6A2*	0.452	0.0025
1416367_at	*C7orf55*	0.452	0.0008
1447713_at	*Tpm1*	0.458	0.0041
1438639_x_at	*EXOC3L2*	0.459	0.0080
1451553_at	*ART5*	0.461	0.0030
1443632_at	*OBSCN*	0.467	0.0153
1452800_a_at	*APOO*	0.467	0.0004
1439332_at	*DDIT4L*	0.471	0.0143
1458369_at	*Atcayos*	0.476	0.0120
1427400_at	*LBX1*	0.476	0.0034
1439352_at	*TRIM7*	0.476	0.0295
1448429_at	*GYG1*	0.477	0.0012
1438378_at	*Med9os*	0.478	0.0043
1416313_at	*MLLT11*	0.478	0.0030
1425274_at	*ASPH*	0.484	0.0216
1434800_at	*SV2B*	0.484	0.0009
1418062_at	*EEF1A2*	0.485	0.0043
1439836_at	*ASB15*	0.486	0.0053
1437947_x_at	*VDAC1*	0.486	0.0006
1438422_at	*LRRC20*	0.487	0.0050
1423025_a_at	*SCHIP1*	0.487	0.0007
1444178_at	*Gm9895*	0.489	0.0022
1449416_at	*FZD4*	0.490	0.0090
1436867_at	*SRL*	0.490	0.0092
1429146_at	*SVIP*	0.492	0.0016
1416455_a_at	*CRYAB*	0.495	0.0162
1448589_at	*NDUFB5*	0.495	0.0002
1418439_at	*MRPL42*	0.496	0.0001
1418413_at	*CAV3*	0.498	0.0056
1418453_a_at	*ATP1B1*	0.500	0.0066
1456859_at	*KIAA1715*	0.500	0.0030

Table S7. Transendothelial migration signature genes down-regulated in endothelium from denervated compared with control paws

Gene name	Fold change denervated vs. control	*P* value
Cd34	0.401	0.017
Axl	0.47	0.167
LOC433749	0.502	0.068
Jam2	0.515	0.009
Cxcl9	0.528	0.288
C3	0.573	0.372
Rhoa	0.575	0.024
2900073G15Rik	0.609	0.081
Icam2	0.609	0.193
Aoc3	0.612	0.253
Stab1	0.629	0.280
Cyba	0.635	0.284
Rock1	0.641	0.082
Myl9	0.646	0.058
Csf1	0.701	0.227
Tgm2	0.721	0.431
Vcam1	0.723	0.561
Rapgef3	0.742	0.352
Lsp1	0.791	0.671
Esam1	0.81	0.118
Pik3r2	0.813	0.176
AI462064	0.817	0.200
Actg1	0.827	0.413
Ccl4	0.833	0.122
Vil2	0.836	0.214
Rassf5	0.861	0.681
Cdh5	0.862	0.512
Abl1	0.864	0.142
Enpp2	0.864	0.469
Vcl	0.866	0.478
Trio	0.869	0.044
Pparg	0.873	0.734
Rac1	0.88	0.757
Actn1	0.882	0.354
Mylc2b	0.883	0.508
Cd99l2	0.904	0.330
Vasp	0.904	0.616
Plcg2	0.911	0.352
Ctnna1	0.913	0.608
F11r	0.937	0.560
Ctnnb1	0.938	0.693
Gnai3	0.942	0.839
Rock2	0.948	0.799
Selpl	0.951	0.581
Cdc42	0.954	0.913
Gnai2	0.96	0.772
Cldn5	0.962	0.917
Actn4	0.972	0.878
D430034N21	0.98	0.833
Msn	0.981	0.584
Mapk12	0.984	0.902
Itgav	0.996	0.989
Prkar1b	1.036	0.832
Pik3ca	1.041	0.844
Mapk11	1.056	0.733
2410026K10Rik	1.086	0.703
Cttn	1.09	0.465
Pxn	1.133	0.447
Itgb3	1.142	0.403
Mapk14	1.165	0.336

Table S7. Cont.

Gene name	Fold change denervated vs. control	*P* value
Pvrl2	1.165	0.583
Ldlr	1.166	0.675
Selp	1.175	0.441
Gnai1	1.181	0.367
Mmp2	1.229	0.548
Bcar1	1.236	0.396
Cd44	1.253	0.567
Pscdbp	1.28	0.526
Ptpn11	1.299	0.250
Ptk2	1.333	0.337
Mmp14	1.543	0.299
Arhgap5	1.57	0.368

Gene sets involved in transendothelial migration/leukocyte extravasation were obtained from the Gene-Set Enrichment Analysis (GSEA) Molecular Signature Database and Ingenuity database.